Search for Long-duration Gravitational-wave Signals Associated with Magnetar Giant Flares

A. Macquet[1] , M. A. Bizouard[1] , E. Burns[2] , N. Christensen[1] , M. Coughlin[3] , Z. Wadiasingh[4,5] , and G. Younes[6,7]

[1] Artemis, Université Côte d'Azur, Observatoire de la Côte d'Azur, CNRS, Nice F-06300, France
[2] Department of Physics & Astronomy, Louisiana State University, Baton Rouge, LA 70803, USA
[3] School of Physics and Astronomy, University of Minnesota, Minneapolis, MN 55455, USA
[4] NASA Goddard Space Flight Center, 8800 Greenbelt Road, Greenbelt, MD 20771, USA
[5] Universities Space Research Association, Columbia, MD 21046, USA
[6] Department of Physics, The George Washington University, Washington, DC 20052, USA
[7] Astronomy, Physics, and Statistics Institute of Sciences (APSIS), The George Washington University, Washington, DC 20052, USA

Abstract

Magnetar giant flares are rare and highly energetic phenomena observed in the transient sky whose emission mechanisms are still not fully understood. Depending on the nature of the excited modes of the magnetar, they are also expected to emit gravitational waves (GWs), which may bring unique information about the dynamics of the excitation. A few magnetar giant flares have been proposed to be associated with short gamma-ray bursts. In this paper we use a new gravitational-wave search algorithm to revisit the possible emission of GWs from four magnetar giant flares within 5 Mpc. While no gravitational-wave signals were observed, we discuss the future prospects of detecting signals with more sensitive gravitational-wave detectors. In particular, we show that galactic magnetar giant flares that emit at least 1% of their electromagnetic energy as GWs could be detected during the planned observing run of the LIGO and Virgo detectors at design sensitivity, with even better prospects for third-generation detectors.

Unified Astronomy Thesaurus concepts: Gravitational waves (678); Gamma-ray bursts (629); Magnetars (992)

1. Introduction

Magnetars, highly magnetized young neutron stars with surface fields often surpassing $>10^{14}$ G, are known to exhibit rare extraordinary flares characterized by micro-to-millisecond gamma-ray flashes of energies 10^{44}–10^{47} erg (isotropic-equivalent) followed by quasi-thermal pulsing tails at $\sim 10^{44}\,\mathrm{erg\,s^{-1}}$ lasting hundreds of seconds. These magnetar giant flares are, in terms of energy, the most extreme phenomena known from isolated neutron stars. Giant flares, and other magnetar phenomenology, are thought to be powered from magnetic free energy stored internally, a reservoir up to $\sim 10^{48}$–10^{49} erg—for reviews, see, e.g., Mereghetti (2008), Turolla et al. (2015). The recent observation of GRB 200415a in the NGC 253 galaxy at 3.57 Mpc (Svinkin et al. 2021) has regenerated much discussion as to magnetar giant flares being a distinct class of short gamma-ray bursts. Its temporal and spectral uniqueness as well as the spatial coincidence with the nearby Galaxy NGC 253 results in a high likelihood of a magnetar giant flare origin. GRB 051103 and GRB 070201 are very likely also magnetar giant flares and a recent analysis of all these events shows that GRB 070222 is probably also of this class (Burns et al. 2021). The four GRBs noted above are all within 5 Mpc, implying a giant flare volumetric rate several orders of magnitude higher than compact object mergers (Burns et al. 2021). The large potential energy release at a relatively nearby distance might make these objects observable with gravitational waves (GWs; Ioka 2001; Corsi & Owen 2011; Quitzow-James et al. 2017), especially with third-generation GW detectors (Kalogera et al. 2019).

GW searches using initial LIGO (Abbott et al. 2009) data have previously been undertaken to look for events coincident with GRB 051103 (Abadie et al. 2012), GRB 070201 (Abbott et al. 2008), and GRB 070222 (Aasi et al. 2014). No GW signals were observed and limits were set. Likewise, limits have also been set for more common and lower-energy magnetar short bursts from six galactic sources (Abadie et al. 2011), among which SGR 1806–20 and SGR 1900+14 are suspected to have had giant flares in the past (Palmer et al. 2005; Hurley et al. 1999). A limit of 2.1×10^{44} erg has been set on the GW energy emitted by SGR 1806–20 for three of the short bursts that occured during the Advanced LIGO's second observing run (Abbott et al. 2019).

A binary neutron-star merger in M81 was excluded as the source of GRB 051103 from the lack of a GW counterpart within a $[-5, +1]$ s window around the gamma-ray-burst time (Abadie et al. 2012). Two un-modeled short-duration (<1 s) transient *burst* searches were also conducted, FLARE with a $[-2, +2]$ s window (Kalmus et al. 2007), and X-PIPELINE with a $[-120, +60]$ s window (Sutton et al. 2010). Assuming M81 as the source, the best upper limits for the emitted GW energy E_{GW} from FLARE were 2.0×10^{51} erg at 100–200 Hz for signals of 100 ms, and an f-mode upper limit of 1.6×10^{54} erg for ringdown signals at 1090 Hz. The X-PIPELINE limits for E_{GW} were 1.2×10^{52} erg at 150 Hz and 6.0×10^{54} erg at 1000 Hz.

For GRB 070201, and assuming M31 as the host, a compact binary merger was also excluded. A search of short-duration (up to 0.1 s) GW bursts was done via a cross-correlation analysis looking for signals within a window of $[-120, +60]$ s. An upper limit on E_{GW} for GW emission for bursts was set at 7.9×10^{50} erg at 150 Hz (Abbott et al. 2008).

GRB 070222 is assumed to come from M83, at a distance of 4.6 Mpc. The previous analysis of LIGO data excluded a binary

neutron-star merger origin out to a distance of 6.7 Mpc. For short bursts (<1 s), X-PIPELINE (Sutton et al. 2010) was used, with a [−600, +60] s window. An exclusion distance was set at 8.9 Mpc for bursts at 150 Hz and 3.5 Mpc for bursts at 300 Hz (Aasi et al. 2014).

Given the importance of the identification of these events as coming from magnetar giant flares, we revisit these events with a new un-modeled GW transient search pipeline, targeting long (≳10 s) and short (∼0.1–1 s) signals. GRB 200415a happened after the Advanced LIGO (Aasi et al. 2015)—Advanced Virgo (Acernese et al. 2015) observing run O3 was suspended, although there are data from GEO-HF (Dooley et al. 2016) and KAGRA (Aso et al. 2013) which were observing at the time. In this paper, we estimate the sensitivity of the Advanced LIGO—Advanced Virgo network to an event like GRB 200415a at O3 and design (O5) sensitivity (Abbott et al. 2020). The results of a search for a GW counterpart to GRB 200415a in GEO-HF and KAGRA data will be reported in a forthcoming publication of the LIGO-Virgo-KAGRA collaboration.

Section 2 presents a description of magnetar giant flares and associated GW emission. The method by which we search for GWs associated with GRB 051103, GRB 070201, and GRB 070222 is given in Section 3. The results of the GW search are presented in Section 4. We discuss the implications of our results in Section 5.

2. Magnetar Giant Flares and Global Stellar Oscillations

The pulsating tails from the three nearest magnetar giant flares are consistent with adiabatically cooling fireballs whose black-body radii are commensurate with typical neutron-star radii. As such, this phenomenology is highly indicative of disruptive activity associated with the inner magnetosphere or crust of the magnetar. Moreover, quasiperiodic oscillations (QPOs) with frequencies ∼20–600 Hz (with one candidate also at 1840 Hz) imprinted on the tail light curves of two giant flares have been reported (Israel et al. 2005; Strohmayer & Watts 2005, 2006; Watts & Strohmayer 2006, 2007). These QPOs are the strongest evidence of nonradial, global, free oscillations of the neutron stars and offer the prospect of astroseismology (Andersson & Kokkotas 1998; Glampedakis & Gualtieri 2018) in both the electromagnetic and GW sectors. For SGR 1806–20, the low-frequency QPOs were initially thought to be long-lived, lasting tens or hundreds of seconds, yet reanalyses by Huppenkothen et al. (2014b) and Miller et al. (2019) have shown the frequencies damp on a short timescale <1 s and are consistent with $n = 0$ crustal torsional or shear modes that are continually re-excited but damp from coupling to the core. This phenomenology is consistent with the theory that predicts such shear modes couple more efficiently to the magnetosphere (Blaes et al. 1989; D'Angelo & Watts 2012; Gabler et al. 2014; Bretz et al. 2021) to produce detectable electromagnetic signals (Timokhin et al. 2008).

Nevertheless, the identification of the QPOs with known modes of neutron stars is still unclear. The low-frequency $n = 0$ crustal torsional or shear modes likely do not couple strongly with GWs, partly because the crust comprises only a few percent of the neutron-star mass. It is not clear if other modes, potentially stronger GW emitters, are excited but are unobserved in the electromagnetic sector due to weaker coupling with the magnetosphere. If the trigger for giant flares is internal (e.g., Thompson & Duncan 1995; Duncan 1998; Ioka 2001; Thompson & Duncan 2001; Gill & Heyl 2010; Lander et al. 2015; Thompson et al. 2017) rather than magnetospheric (e.g., Lyutikov 2003; Komissarov et al. 2007;

Parfrey et al. 2012),[8] many possible resonant modes in the core and crust of the magnetar may be excited during giant flares depending on the nature and details of the trigger mechanism. Some of these modes, such as f-modes and g-modes, may also produce GWs, though current models indicate that they will be too weak to be detected (Levin & van Hoven 2011; Zink et al. 2012). The upper limit for GW emission is ultimately derived from the magnetic free-energy reservoir and may exceed ≳10^{48} erg (Ioka 2001; Corsi & Owen 2011).

Given all the uncertainties about magnetar giant flare triggering mechanisms and the local source and its possible GW emission, in the following, we conduct un-modeled GW searches with a large parameter space; we assume that the GW signal could be as short as ∼.1 s, repeating or not over a few hundred seconds or as long-lived as ∼500 s with a frequency range that goes up to 2 kHz.

3. Search Methodology

Our sample contains four GRBs for which a likely magnetar giant flare origin has been identified. For three of them, GRB 051103 (Golenetskii et al. 2005; Hurley et al. 2010), GRB 070201 (Golenetskii et al. 2007; Hurley et al. 2007), and GRB 070222 (Svinkin et al. 2016; Burns et al. 2021), coincident data from two of the three initial LIGO detectors (H1, H2, and L1) are available from the fifth science run (S5) from 2005 to 2007. The Virgo detector first science run (VSR1) had not started at the time of these three GRBs. GRB 200415a (Fermi GBM Team 2020; Svinkin et al. 2020) was observed after the Advanced LIGO and Advanced Virgo detectors had completed their third observing run (O3). Only KAGRA (K1) and the GEO-HF (G1) detectors were acquiring data at the time of the GRB. A publication by the LIGO–Virgo–KAGRA collaboration including GRB 200415a is in preparation. We have thus not analyzed GRB 200415a, but have considered it for a prospective study to estimate the chance of detecting a GW signal when advanced GW detectors will reach their design sensitivity, expected during S5 (Abbott et al. 2020).

Two distinct searches are performed for each event, one targeting short-duration signals (∼0.1–1 s) and another that is best suited for signals with longer duration (∼10–500 s). The time interval used to analyze the data for each search is referred to as the *on-source* window. As the time delay between gamma-ray and potential GW emission is not precisely constrained (Zink et al. 2012), we choose a large interval of 512 s on both sides of the GRB trigger time t_0. We also define an *off-source* window that consists of an interval of data close to (but outside of) the on-source window. These data are used to estimate the background trigger distribution and the sensitivity of the search. Both the on-source and off-source windows are split into windows of duration 512 s that correspond to the maximal duration of the expected GW signal with 50% overlap to optimize computational efficiency. For each type of search, and each of the GRBs, whose main characteristics are given in Table 1, LIGO GW data are searched with the algorithm described below.

The GW signal is searched by cross-correlating strain data from two detectors. This method is well suited for

---

[8] Note that the original instability timescale estimates in Lyutikov (2003) for the relativistic tearing instability mechanism were erroneous and corrected by Elenbaas et al. (2016). This re-examination found much shorter minimum timescales (for plausible magnetospheric parameters), commensurate with the observed rise time of giant flares.

Table 1
A Summary of the Magnetar Giant Flare Samples and Detectors That Were Observed at the Time of Each Event

Event	Time (UTC)	Host	Distance (Mpc)	Detectors	Pair Efficiency
GRB 051103	09:25:42 UTC 3 November 2005	M81	3.6	H2, L1	0.47
GRB 070201	15:23:10 UTC 1 February 2007	M31	0.77	H1, H2	0.30
GRB 070222	07:31:55 UTC 22 February 2007	M83	4.6	H1, H2	0.32
GRB 200415a	08:48:05 UTC 15 April 2020	NGC 253	3.3	G1, K1	0.47[a]

Notes. Pair efficiency is based on the quadrature sum of the detectors' antenna factors and characterizes the detectors' network sensitivity to a GW signal coming from a given direction (see Thrane et al. 2011).
[a] Computed for the (H1, L1) pair.

long-duration GW signals whose waveform is unknown. We use the PySTAMPAS pipeline (A. Macquet et al. 2021, in preparation), a new python pipeline designed to search for long-duration GW signals in interferometric detectors, based on the Matlab-based STAMP pipeline (Thrane et al. 2011). The pipeline parameter space searches for GW signals between 30 and 2000 Hz lasting from a few to ∼500 s in the long-duration configuration, or ∼1 s when tuned to search for shorter signals.

The data from each detector are first high-pass-filtered with a frequency cutoff at 22 Hz to remove most of the low-frequency content of the detectors' strain data. A gating algorithm is applied to remove high-amplitude, short-duration spikes that are often present in the data (Davis et al. 2021). A time-frequency map (ft-map) is built using the Fourier transform of short segments of duration 1 s, which are Hann-windowed and overlap by 50%. The frequency range of the maps is 30–2000 Hz. The ft-maps are whitened by the one-sided amplitude spectral density, which is estimated by taking the median of the squared modulus of the Fourier transform over 20 adjacent frequency bins. This estimator for the amplitude spectral density maximizes the sensitivity to monochromatic and quasi-monochromatic signals, yet GW detector data contain narrow and high-amplitude spectral artefacts that have an instrumental origin (mechanical resonances and power lines, among others; Davis et al. 2021). As these lines can be easily mistaken for monochromatic GW signals, it is necessary to identify and remove the main ones. This is done using the off-source window data. For each window, frequency bins whose mean value over a map exceed a threshold of 2 (the pixel's values follow a χ^2 with 2 degrees of freedom) are listed as "potential instrumental lines." If, in addition, these potential instrumental lines are persistent in more than 5% of the total time of the off-source window, all the pixels corresponding to that frequency are set to 0 ("notched") for all ft-maps. Overall, ∼5% of the total frequency bins are notched for each search.

A seed-based clustering algorithm is then run over the single-detector ft-maps to identify groups of pixels with absolute value above a given threshold (Prestegard 2016). The parameters of the clustering algorithm are tuned according to the type of signals searched. For long-duration signals, the energy is expected to be spread over several pixels, so we set a low threshold on the individual pixels' power (incoherent energy) and dismiss clusters that contain less than 20 pixels. The opposite approach is taken for short-duration signals. Because the energy is typically concentrated in only a few pixels, we do not apply a constraint on the number of pixels in a cluster, but we increase the threshold on pixels' incoherent energy to reduce the number of noise clusters.

The extracted clusters are cross-correlated with the other detector's pixels to compute a coherent signal-to-noise ratio (S/N). This computation takes into account the phase shift induced by the delay of arrival time of a GW signal in the two detectors, which depends on the source's position for spatially separated detectors. We consider the center of the error box given in Golenetskii et al. (2005), Hurley et al. (2007), and Burns et al. (2021) for GRB 051103, GRB 070201, and GRB 070222, respectively. An error over the source position induces a loss of S/N for the non-co-located detectors' pair, which depends on the distance between the detectors and the GW signal frequency. For GRB 051103, considering the area of the error box on the position of 120 squared arcminutes (Golenetskii et al. 2005), the maximal loss of S/N would be ∼8% considering a GW signal at 2000 Hz. Coherent pixels are grouped to form a *trigger*. Each trigger is assigned a detection statistic p_Λ based on its pixels' S/N and the incoherent energy in each detector's data (A. Macquet et al. 2021, in preparation). This hierarchical approach allows us to perform the analyses much faster as cross-correlation is computed only for a small subset of pixels without sacrificing sensitivity (Thrane & Coughlin 2015). To assess the significance of triggers found in the on-source window, we estimate the distribution of background triggers due to the detectors' noise. To ensure that the data do not contain any coherent GW signal, the data streams of the two detectors are shifted with respect to each other by at least 256 s, which is much larger than the light travel time between the detectors. The data are analyzed identically to that of the on-source window and this process is repeated for several timeshifts to simulate multiple instances of the noise. The cumulative rate of triggers provides an estimation of the false-alarm rate (FAR) that we use to determine the detection threshold on p_Λ for the on-source window analysis. The FAR distributions obtained for each GRB are shown in Figure 1. The number of background triggers is different for each GRB. This is especially true for GRB 051103, which occurred at the very beginning of S5, when many sources of noise were not yet mitigated. Since loud noise triggers that populate the tail of the distributions are often due to noise fluctuations in one detector, we suppress them by requiring that the S/N ratio between the detectors be lower than 10. The same cut is applied for the coincident analysis and efficiency estimation. Using these results we choose a detection threshold p_Λ corresponding to a FAR of ∼1/20 yr^{-1}. Assuming a Poissonian distribution for noise events, this corresponds to a false-alarm probability in the on-source window of ∼10^{-6}.

We estimate the detection efficiency of the searches by adding simulated signals into the data. The waveforms injected are chosen to cover the parameter space constrained by the potential processes of emission described in Section 2. We use sinusoidal signals multiplied by a decaying exponential function (damped sine) to simulate damped, quasi-monochromatic GW emission. For long-duration searches, decay times and central frequencies of
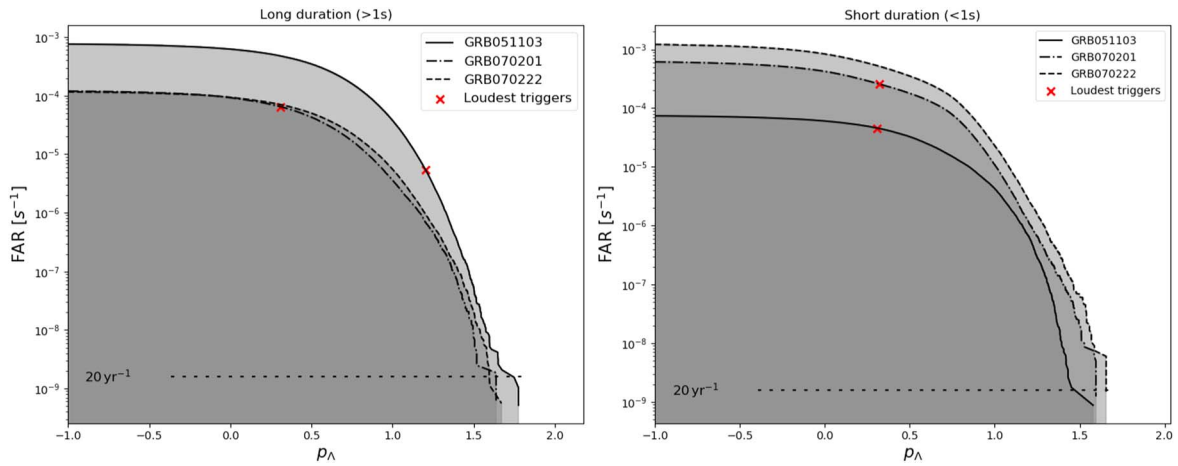
Figure 1. Cumulative distribution of background noise triggers for each GRB on top of which crosses represent the GW triggers found in the on-source windows of GRB 051103 and GRB 070201. No trigger has been found for GRB 070222. The left and right panels show the results of long-duration and short-duration searches, respectively.

the waveforms are varied between 2–10 s and 50–500 Hz, respectively. Short-duration searches use a damped sine with 0.2 s decay time and a mean frequency of 100 Hz. Note that the potential GW emission of MGF may be more complex than a damped sinusoid. However, since the detection method relies on a cross-correlation, the sensitivity of the search mainly depends on the frequency, duration, and energy of the signal. Given the large parameter space and the lack of precisely modeled waveforms, we limit our models to damped sinusoids, which provide a good estimation of the sensitivity of the search. For each waveform, we generate 100 random starting times uniformly distributed inside the off-source window. The strain response of both detectors is computed using antenna factors and time delays that correspond to the time and location of the targeted GRB. Since the orientation of the source is unknown, we draw random values uniform in the GW polarization angle and the cosine of the source's inclination angle. The simulated signals are added to the data and analyzed by the search algorithm. A signal is considered recovered if a trigger is found within the time and frequency boundaries of the simulated signal, and with a statistic p_Λ higher than the detection threshold corresponding to our choice of $1/20 \, \text{yr}^{-1}$. This process is repeated for different signal amplitudes to estimate the detection efficiency of the search.

4. Results

The searches for GW signals in each GRB on-source window identified triggers; their FAR is then compared to the background estimation in Figure 1. Table 2 summarizes the characteristics of the loudest event for each GRB and each type of search. Further analysis of these triggers shows that their FARs fit well within the core of the background distribution and their morphological properties match those of noise triggers or spectral lines. None of the triggers have a FAR lower than the detection threshold that we fixed at $1/20 \, \text{yr}^{-1}$. We therefore report that no confident GW signal has been found in any of the GRB on-source windows in either the long- or short-duration searches.

We then use the results of efficiency studies to place upper limits on the emitted GW energy. Considering the distance to the GRBs given by the host galaxy, one can compute the isotropic GW energy radiated by a source at distance r

assuming a quadrupolar emission:

$$E_{\text{GW}} = r^2 \frac{c^3}{4G} \int (\dot{h}_+^2(t) + \dot{h}_\times^2(t)) dt. \quad (1)$$

where $h_+(t)$ and $h_\times(t)$ are the polarisations of the GW signal. We use the simulated waveforms added to the data described in Section 3 to estimate the energy corresponding to a detection efficiency of 50% at a FAR of $1/20 \, \text{yr}^{-1}$. These values correspond to the minimal GW energy we are able to detect in the data for each GRB. This GW energy limit is then compared to the estimation of the isotropic-equivalent electromagnetic energy of the events E_{iso} summarized in Burns et al. (2021). All values are given in Table 3. The upper limits on E_{GW} are several orders of magnitude higher than E_{iso} and therefore do not provide meaningful constraints over the ratio of GW energy to the electromagnetic energy emitted. These results can be compared with the ones established by previous searches for short-duration GW emission around GRB 051103 (Kalmus et al. 2007; Sutton et al. 2010), GRB 070201 (Abbott et al. 2008), and GRB 070222 (Aasi et al. 2014). Overall, we report a sensitivity increase by a factor ∼2 compared to upper limits set with the X-PIPELINE. For GRB 051103, FLARE-reported upper limits are ∼4 times lower than those obtained with PySTAMPAS. The discrepancy could be explained by the fact that we use a more conservative detection threshold than FLARE, which used the FAR of the loudest event in the on-source window as a detection threshold. Furthermore, the FLARE search was sensitive to only narrowband and short-duration (<100 ms) GW signals. PySTAMPAS covers a larger parameter space (in duration and bandwidth) and is sensitive to a large variety of signal morphologies.

In addition to the three GRBs analyzed using S5 data, we also performed a sensitivity study for GRB 200415a using simulated data following H1 and L1 sensitivity at the end of O3 (Goetz 2020a, 2020b) to estimate what would have been the chance to detect GW emission from this source if the Advanced detector network was still observing in 2020 April. The gain of more than two orders of magnitude observed for this GRB E_{GW} limit is mainly due to the LIGO detectors' sensitivity gain

Table 2
Properties of the Loudest Triggers Found in Each GRB On-source Window for Long-duration and Short-duration Searches

GRB	Search	$t_{start} - t_0$ (s)	Duration (s)	Frequency Range (Hz)	FAP
GRB 051103	Long	286	8	1640–1642	5.5×10^{-3}
	Short	91	2.5	249–251	2.0×10^{-1}
GRB 070201	Long	158	12	237–243	6.4×10^{-2}
	Short	431	1	783–786	4.8×10^{-1}

Note. t_{start} refers to the starting time of the GW trigger, while t_0 is the GRB trigger time. The false-alarm probability (FAP) is inferred from the FAR and the duration of the on-source window.

Table 3
GW Energy Emitted for a Source Detected at 50% Efficiency for an FAP of 10^{-6}

Duration (s)	f_0 (Hz)	GW Energy Limits (erg)			
		GRB051103	GRB070201	GRB070222	GRB200415a
0.2	100	1.44×10^{52}	3.47×10^{50}	1.69×10^{52}	2.3×10^{49}
2	100	5.95×10^{51}	3.07×10^{50}	9.19×10^{51}	1.43×10^{49}
2	250	2.56×10^{52}	8.83×10^{50}	5.56×10^{52}	1.21×10^{50}
2	500	3.32×10^{53}	1.25×10^{52}	7.13×10^{53}	…
10	100	6.70×10^{51}	2.36×10^{50}	1.24×10^{52}	1.53×10^{49}
10	250	3.22×10^{52}	1.35×10^{51}	6.30×10^{52}	1.14×10^{50}
10	500	4.13×10^{53}	1.69×10^{52}	9.11×10^{53}	…
		Isotropic-equivalent EM energy E_{iso} (erg)			
		5.3×10^{46}	1.6×10^{45}	6.2×10^{45}	1.3×10^{46}

Note. These limits are obtained considering damped sine signals whose parameters range a large portion of the parameter space. Limits for [0.2] s emission have been obtained in the short-duration configuration of the pipeline. Values for GRB 200415a have been obtained using the last 15 days of data from O3 taken by LIGO in March 2020. We do not report values at 500 Hz for GRB 200415a as this frequency is notched because of a mechanical resonance in H1 and L1 during O3. The isotropic electromagnetic energy E_{iso} of each event computed by Burns et al. (2021) is given for comparison.

between S5 and O3. That gain would have allowed us to constrain the GW energy emitted to $E_{GW} \lesssim 10^{3-4} E_{iso}$.

Finally, to estimate the detection sensitivity that will be achievable in the future, we used simulated data following Advanced LIGO's design sensitivity (expected during the O5 run), and the sensitivity of a proposed third-generation GW detector, the Einstein Telescope (Hild et al. 2011), which is expected to be in a network with the US-led Cosmic Explorer (Reitze et al. 2019). As the detectors' network sensitivity depends on the direction of the GW source, waveforms have been injected at random positions to simulate a generic magnetar giant flare source. In this study, we used the Einstein Telescope, treated as two co-located interferometric detectors whose arms form a 60° angle and arbitrarily located in Italy, but similar results would have been obtained with two Cosmic-Explorer-like detectors in the US. We summarize all these results in Figure 2 and compare the inferred upper limits on the GW energy detectable to the estimated E_{iso} of the candidate magnetar giant flares as a function of the source's distance. Upper limits on the GW energy decrease by a factor ∼2 between O3 and O5, which is compatible with the detector's expected sensitivity gain (Davis et al. 2021). We show that it would be possible to constrain the GW energy emitted up to a fraction of E_{iso} for magnetar giant flares in the Milky Way and in the Magellanic Clouds, in both scenarios of long-duration and short-duration GW emission with Advanced LIGO at design sensitivity. Third-generation detectors such as the Einstein Telescope or Cosmic Explorer should provide a factor ∼100 increase in sensitivity to GW energy, making even less energetic flares from galactic magnetars detectable.

5. Discussion

The recent observation of GRB 200415a, suggesting that magnetar giant flares may be a distinct class of short gamma-ray bursts with a substantially higher volumetric rate than compact object mergers (Burns et al. 2021), has motivated the re-examination of gravitational-wave data around three other likely magnetar giant flare events in nearby galaxies. We used a new GW search pipeline PySTAMPAS (A. Macquet et al. 2021, in preparation), that allows us to cover many possible GW emission mechanisms. Given the large distances to these sources and the typical electromagnetic energy emitted, the prospects of detecting such signals from outside the Milky Way were low, yet substantial and imminent improvements in GW detector sensitivity will enable probing a regime where the GW energy is comparable to or less than the typical magnetar giant flare electromagnetic energy for the first time for extragalactic events. Moreover, future Galactic giant flares may lead to the first detection under the assumption that the GW signal carries >0.1% of the EM energy released with limits down to $\gtrsim 10^{-6}$ for third-generation detectors, which can probe GWs for even the weakly GW-emitting low-frequency torsional modes. For the nearest Galactic magnetars at ∼2 to 4 kpc, third-generation detectors could even begin probing a regime of more common recurrent magnetar short bursts and intermediate flares, which have electromagnetic energies $\lesssim 10^{43}$ erg (Israel et al. 2008), especially during burst forests when repeated excitations are plausible (Younes et al. 2020). Our new pipeline readies us for such an era.

As mentioned in Section 2, the essential trigger of magnetar giant flares is unknown, although many proposals exist (e.g., Ramaty et al. 1980; Thompson & Duncan 1995; Duncan 1998;
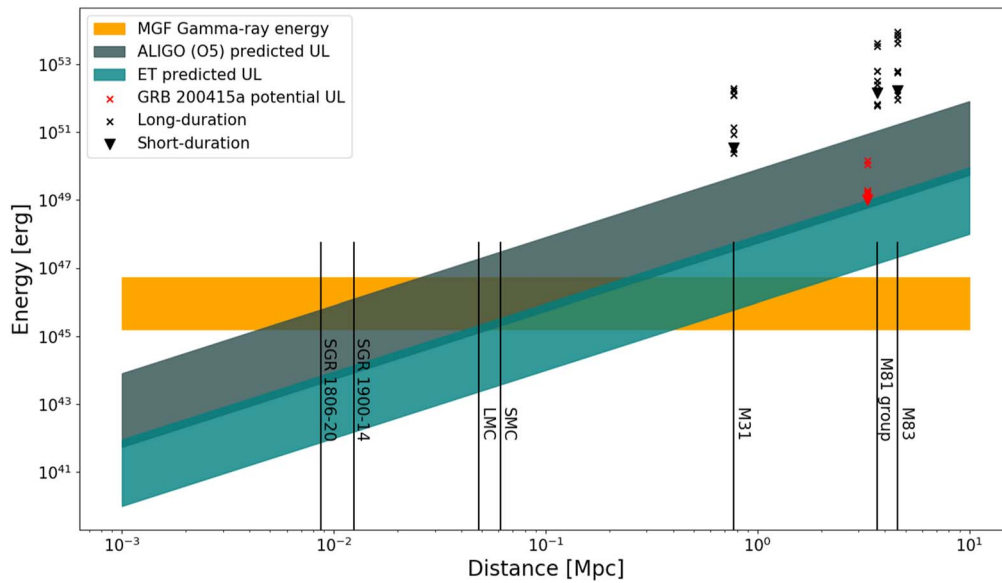
Figure 2. Upper limits (UL) on the GW energy emitted by GRB051103 (M81), GRB070222 (M83), and GRB070201 (M31) during S5 are represented with crosses for long-duration emission and triangles for short-duration emission. Each point corresponds to a different duration/frequency-damped sine-simulated waveform added to the data. For GRB200415a, crosses note the limits that could have been set up for this event with LIGO if it had been observing at the time. The dark gray band and blue band represent the limit on E_{GW} as a function of the distance to the source (averaging over all possible sky positions), which will be achievable with Advanced LIGO data at design sensitivity (O5) and the Einstein Telescope, respectively. The orange band represents the minimal/maximal E_{iso} estimated for the three GRBs analyzed in this study. Distances of nearest galaxies and soft gamma repeaters SGR 1806–20 and SGR 1900–14 are shown for convenience.

Ioka 2001; Thompson & Duncan 2001; Lyutikov 2003; Komissarov et al. 2007; Gill & Heyl 2010; Parfrey et al. 2012; Lander et al. 2015; Elenbaas et al. 2016; Thompson et al. 2017). The high (volumetric) rate of giant flares (Burns et al. 2021), which exceeds the core-collapse supernova rate, implies giant flares may reoccur many times during a magnetar's active lifespan. This disfavors giant flare mechanisms with finality, such as phase transitions (Ramaty et al. 1980), redistribution of stellar structure, and moment of inertia (Ioka 2001), or catastrophic internal magnetic field rearrangements such as the magnetohydrodynamic interchange instability (Thompson & Duncan 1995). These dramatic internal mechanisms may produce GWs with considerable power, possibly comparable to a few percent of the gravitational binding energy of $\sim 10^{53}$ erg. Our limits on the M31 giant flare GRB 070201 encroach on such an energy scale and future limits on nearby giant flares will definitively rule out such energetic scenarios.

Note that the location and nature of the physical trigger mechanism, for instance, whether it is magnetospheric or internal to the neutron star, can influence the character of the global free oscillations and what modes may be excited in a rich but complicated manner that depends on the equation of state and configuration of magnetic fields in the core and crust of the magnetar (Passamonti et al. 2007; Colaiuda et al. 2009; Colaiuda & Kokkotas 2011, 2012; Corsi & Owen 2011; Gabler et al. 2011, 2012; Zink et al. 2012). This can strongly influence the relative apportionment between energy emitted in the gravitational and electromagnetic sectors, particularly if f-modes are excited more efficiently over torsional or shear modes that couple more readily to the magnetosphere for electromagnetic emission (Blaes et al. 1989; Timokhin et al. 2008; Link 2014; Bretz et al. 2021). However, significant theoretical uncertainty also exists on the EM emission locale, radiative processes, photon transport, beaming, and outflows in giant flares (e.g., van Putten et al. 2016) which can muddle firm inferences on the EM energetics. Thus characterization or

constraints on GWs from magnetar activity is essential to understanding the energetics and nature of the unknown trigger (s) and how strongly they couple to the interior of the neutron star. This has implications beyond giant flares, as more common short bursts may also share the same physical trigger and similar QPOs have been reported in those (Huppenkothen et al. 2014a, 2014c). Likewise, the inferred power-law energy distribution of giant flares reported by Burns et al. (2021) is consistent with the recurrent short-burst distribution observed in Galactic magnetars, suggesting a continuum of burst energies and a similar trigger for both lower-energy recurrent short bursts and giant flares. Recent unprecedented results from NICER of SGR 1830–0645 (Younes et al. submitted) also reveal a strong phase dependence of short bursts aligned with the surface thermal emission pulse profile; this would point to a low-altitude trigger, associated with the crust, and might disfavor high-altitude equatorial magnetospheric trigger models. A low-altitude or crustal trigger would perhaps improve prospects for third-generation GW detectors, particularly for limits approaching the level of $\sim 10^{-6}$ of the EM power expected from excited f-modes (Levin & van Hoven 2011). However, given the uncertainties, a nondetection may not be enough to rule out most of the models describing the coupling between the crust and the core. Nevertheless, after the recent association of a fast radio burst with a similar short-burst event (Bochenek et al. 2020; Mereghetti et al. 2020; Li et al. 2021) and proposals that magnetar oscillations may underlie some fast radio bursts (Wadiasingh & Timokhin 2019; Suvorov & Kokkotas 2019; Wadiasingh & Chirenti 2020; Wadiasingh et al. 2020), GW studies offer a potentially unique view on the trigger of magnetar bursts. This also motivates the development of new detection algorithms that more specifically target repeating signals associated with QPOs.

Finally, we note that the volumetric high rate of magnetar giant flares inferred by Burns et al. (2021) potentially allows for a nonnegligible contribution to the stochastic GW background

(Christensen 2019) by mature magnetars, likely pertinent for third-generation detectors such as the Einstein Telescope (Hild et al. 2011) and Cosmic Explorer (Reitze et al. 2019). This will be investigated in a future study.

ORCID iDs

A. Macquet ● https://orcid.org/0000-0001-5955-6415
M. A. Bizouard ● https://orcid.org/0000-0002-4618-1674
E. Burns ● https://orcid.org/0000-0002-2942-3379
N. Christensen ● https://orcid.org/0000-0002-6870-4202
M. Coughlin ● https://orcid.org/0000-0002-8262-2924
Z. Wadiasingh ● https://orcid.org/0000-0002-9249-0515
G. Younes ● https://orcid.org/0000-0002-7991-028X

References

Aasi, J., Abbott, B., Abbott, R., et al. 2014, PhRvL, 113, 011102
Aasi, J., Abbott, B. P., Abbott, R., et al. 2015, CQGra, 32, 074001
Abadie, J., Abbott, B., Abbott, T., et al. 2012, ApJ, 755, 2
Abadie, J., Abbott, B. P., Abbott, R., et al. 2011, ApJL, 734, L35
Abbott, B., Abbott, R., Adhikari, R., et al. 2008, ApJ, 681, 1419
Abbott, B. P., Abbott, R., Abbott, T. D., et al. 2019, ApJ, 874, 163
Abbott, B. P., Abbott, R., Abbott, T. D., et al. 2020, LRR, 23, 3
Abbott, B. P., Abbott, R., Adhikari, R., et al. 2009, RPPh, 72, 076901
Abbott, R., Abbott, T. D., Abraham, S., et al. 2021, SoftX, 13, 100658
Acernese, F., Agathos, M., Agatsuma, K., et al. 2015, CQGra, 32, 024001
Andersson, N., & Kokkotas, K. D. 1998, MNRAS, 299, 1059
Aso, Y., Michimura, Y., Somiya, K., et al. 2013, PhRvD, 88, 043007
Blaes, O., Blandford, R., Goldreich, P., & Madau, P. 1989, ApJ, 343, 839
Bochenek, C. D., Ravi, V., Belov, K. V., et al. 2020, Natur, 587, 59
Bretz, J., van Eysden, C. A., & Link, B. 2021, MNRAS, 504, 5880
Burns, E., Svinkin, D., Hurley, K., et al. 2021, ApJL, 907, L28
Christensen, N. 2019, RPPh, 82, 016903
Colaiuda, A., Beyer, H., & Kokkotas, K. D. 2009, MNRAS, 396, 1441
Colaiuda, A., & Kokkotas, K. D. 2011, MNRAS, 414, 3014
Colaiuda, A., & Kokkotas, K. D. 2012, MNRAS, 423, 811
Corsi, A., & Owen, B. J. 2011, PhRvD, 83, 104014
D'Angelo, C. R., & Watts, A. L. 2012, ApJL, 751, L41

Davis, D., Areeda, J. S., Berger, B. K., et al. 2021, CQGra, 38, 135014
Dooley, K. L., Leong, J. R., Adams, T., et al. 2016, CQGra, 33, 075009
Duncan, R. C. 1998, ApJL, 498, L45
Elenbaas, C., Watts, A. L., Turolla, R., & Heyl, J. S. 2016, MNRAS, 456, 3282
Fermi GBM Team 2020, GCN, 27579, 1
Gabler, M., Cerdá Durán, P., Font, J. A., Müller, E., & Stergioulas, N. 2011, MNRAS, 410, L37
Gabler, M., Cerdá-Durán, P., Stergioulas, N., Font, J. A., & Müller, E. 2012, MNRAS, 421, 2054
Gabler, M., Cerdá-Durán, P., Stergioulas, N., Font, J. A., & Müller, E. 2014, MNRAS, 443, 1416
Gill, R., & Heyl, J. S. 2010, MNRAS, 407, 1926
Glampedakis, K., & Gualtieri, L. 2018, in The Physics and Astrophysics of Neutron Stars, ed. R Luciano et al. (Cham: Springer), 673
Goetz, E. 2020a, H1 Calibrated Sensitivity Spectra Jan 04 2020, Ligo Document Control Center
Goetz, E. 2020b, L1 Calibrated Sensitivity Spectra Jan 04 2020, Ligo Document Control Center
Golenetskii, S., Aptekar, R., Mazets, E., et al. 2005, GCN, 4197, 1
Golenetskii, S., Aptekar, R., Mazets, E., et al. 2007, GCN, 6088, 1
Hild, S., Abernathy, M., Acernese, F., et al. 2011, CQGra, 28, 094013
Huppenkothen, D., D'Angelo, C., Watts, A. L., et al. 2014c, ApJ, 787, 128
Huppenkothen, D., Heil, L. M., Watts, A. L., & Göğüs, E. 2014a, ApJ, 795, 114
Huppenkothen, D., Watts, A. L., & Levin, Y. 2014b, ApJ, 793, 129
Hurley, K., Cline, T., Mazets, E., et al. 1999, Natur, 397, 41
Hurley, K., Goldsten, J., Golenetskii, S., et al. 2007, GCN, 6103, 1
Hurley, K., Rowlinson, A., Bellm, E., et al. 2010, MNRAS, 403, 342
Ioka, K. 2001, MNRAS, 327, 639
Israel, G. L., Belloni, T., Stella, L., et al. 2005, ApJL, 628, L53
Israel, G. L., Romano, P., Mangano, V., et al. 2008, ApJ, 685, 1114
Kalmus, P., Khan, R., Matone, L., & Márka, S. 2007, CQGra, 24, S659
Kalogera, V., Bizourard, M.-A., Burrows, A., et al. 2019, BAAS, 51, 239
Komissarov, S. S., Barkov, M., & Lyutikov, M. 2007, MNRAS, 374, 415
Lander, S. K., Andersson, N., Antonopoulou, D., & Watts, A. L. 2015, MNRAS, 449, 2047
Levin, Y., & van Hoven, M. 2011, MNRAS, 418, 659
Li, C. K., Lin, L., Xiong, S. L., et al. 2021, NatAs, in press
Link, B. 2014, MNRAS, 441, 2676
Lyutikov, M. 2003, MNRAS, 346, 540
Mereghetti, S. 2008, A&ARv, 15, 225
Mereghetti, S., Savchenko, V., Ferrigno, C., et al. 2020, ApJL, 898, L29
Miller, M. C., Chirenti, C., & Strohmayer, T. E. 2019, ApJ, 871, 95
Palmer, D. M., Barthelmy, S., Gehrels, N., et al. 2005, Natur, 434, 1107
Parfrey, K., Beloborodov, A. M., & Hui, L. 2012, ApJL, 754, L12
Passamonti, A., Stergioulas, N., & Nagar, A. 2007, PhRvD, 75, 084038
Prestegard, T. 2016, PhD Thesis, Univ. of Minnesota
Quitzow-James, R., Brau, J., Clark, J. A., et al. 2017, CQGra, 34, 164002
Ramaty, R., Bonazzola, S., Cline, T. L., et al. 1980, Natur, 287, 122
Reitze, D., Adhikari, R. X., Ballmer, S., et al. 2019, BAAS, 51, 035
Strohmayer, T. E., & Watts, A. L. 2005, ApJL, 632, L111
Strohmayer, T. E., & Watts, A. L. 2006, ApJ, 653, 593
Sutton, P. J., Jones, G., Chatterji, S., et al. 2010, NJPh, 12, 053034
Suvorov, A. G., & Kokkotas, K. D. 2019, MNRAS, 488, 5887
Svinkin, D., Golenetskii, S., Aptekar, R., et al. 2020, GCN, 27595, 1
Svinkin, D. S., Frederiks, D. D., Aptekar, R. L., et al. 2016, ApJS, 224, 10
Svinkin, D., Frederiks, D., Hurley, K., et al. 2021, Natur, 589, 211
Thompson, C., & Duncan, R. C. 1995, MNRAS, 275, 255
Thompson, C., & Duncan, R. C. 2001, ApJ, 561, 980
Thompson, C., Yang, H., & Ortiz, N. 2017, ApJ, 841, 54
Thrane, E., & Coughlin, M. 2015, PhRvL, 115, 181102
Thrane, E., Kandhasamy, S., Ott, C. D., et al. 2011, PhRvD, 83, 083004
Timokhin, A. N., Eichler, D., & Lyubarsky, Y. 2008, ApJ, 680, 1398
Turolla, R., Zane, S., & Watts, A. L. 2015, RPPh, 78, 116901
van Putten, T., Watts, A. L., Baring, M. G., & Wijers, R. A. M. J. 2016, MNRAS, 461, 877
Wadiasingh, Z., Beniamini, P., Timokhin, A., et al. 2020, ApJ, 891, 82
Wadiasingh, Z., & Chirenti, C. 2020, ApJL, 903, L38
Wadiasingh, Z., & Timokhin, A. 2019, ApJ, 879, 4
Watts, A. L., & Strohmayer, T. E. 2006, ApJL, 637, L117
Watts, A. L., & Strohmayer, T. E. 2007, AdSpR, 40, 1446
Younes, G., Güver, T., Kouveliotou, C., et al. 2020, ApJL, 904, L21
Zink, B., Lasky, P. D., & Kokkotas, K. D. 2012, PhRvD, 85, 024030